# Excitation into $3p^5 5p$ levels from the metastable levels of Ar

R. O. Jung, John B. Boffard, L. W. Anderson, and Chun C. Lin
*Department of Physics, University of Wisconsin, Madison, Wisconsin 53706, USA*
(Received 25 January 2007; published 11 May 2007)

Measurements of cross sections for electron-impact excitation out of the $J=0$ and $J=2$ $3p^5 4s$ metastable levels of argon into nine of the ten levels of the $3p^5 5p$ manifold are presented in the energy range from threshold to 10 eV. A mixed target of atoms in both metastable levels was created by a hollow cathode discharge. Laser quenching was used to depopulate either one of the metastable levels, allowing separate measurements of the cross sections from each of the two metastable levels. Unlike the metastable excitation cross sections into $3p^5 4p$ levels, the cross sections into the $3p^5 5p$ levels are not found to be proportional to optical oscillator strengths.

DOI: 10.1103/PhysRevA.75.052707 PACS number(s): 34.80.My, 34.80.Dp, 52.20.Fs

## I. INTRODUCTION

### A. Motivation

Electron-impact excitation cross sections are of great interest for both furthering the understanding of fundamental collisions physics, as well as for practical applications such as plasma diagnostics. Collisions between electrons and rare-gas atoms in metastable levels are of particular interest since these collision processes share similarities with two of the most widely studied systems: excitation from the ground states of the rare gases and alkalis. Consider excitation into the levels of the Ar($3p^5 4p$) manifold. Electron-impact excitation into these levels from the Ar($3p^6$) ground state requires a minimum electron energy of about 13 eV, with typical peak cross sections on the order of $10^{-18}$ cm$^2$ [1]. In contrast, excitation cross sections into these same levels from the Ar($3p^5 4s$) metastable levels are as large as $10^{-15}$ cm$^2$ with excitation thresholds of only 1.5 eV [2]. While the final state atomic wave functions are the same in the two cases, the dynamics of the active electron in the $3p \rightarrow 4p$ ground state excitation process are quite different than the $4s \rightarrow 4p$ metastable excitation process. A better correspondence, however, is provided by viewing the $4s \rightarrow 4p$ excitation from the standpoint of excitation out of the ground state of potassium [3]. Indeed, in terms of the energy thresholds, peak values, and general energy dependencies, the K($4s \rightarrow 4p$) and Ar($3p^5 4s \rightarrow 3p^5 4p$) cross sections bear a closer resemblance to one another than the Ar($3p^6 \rightarrow 3p^5 4p$) and Ar($3p^5 4s \rightarrow 3p^5 4p$) cross sections do. Thus, by comparing results for excitation from the ground state and metastable levels we can glean information on the sensitivity of cross sections to both the atomic structure of the target and the collision process.

Previous measurements on the excitation from the $np^5(n+1)s$ metastable levels of Ne-Xe ($n=2-5$) to levels of the $np^5(n+1)p$ configuration have revealed three general patterns [4]; of these, two are related to changes in the quantum numbers of the initial and final levels, namely $J$ the total angular momentum, and $j_c$ the angular momentum of the $np^5$ core (see Sec. I B). The first pattern is that excitation cross sections corresponding to dipole-allowed excitation processes ($\Delta J = \pm 1, 0$ with $J=0 \not\rightarrow 0$) are larger than the cross sections for dipole-forbidden excitations, and have a weaker dependence on the incident electron energy [2,5]. The second pattern, which is evident only in the heaviest rare gases (Kr and Xe), is that excitation cross sections that preserve the core angular momentum ($\Delta j_c = 0$) are larger than core-changing cross sections [6]. In Xe (or Kr) the spin-orbit coupling of the $5p^5$ (or $4p^5$) core is much stronger than the coupling between the core and the outer electron so that the core angular momentum is a good quantum number. In contrast, the Ar($3p^5$) core has a much weaker spin-orbit coupling, which is disengaged by the much stronger Coulomb perturbation due to the outer $4p$ electron, hence it is not physically meaningful to speak of $j_c$ for the Ar $3p^5 4p$ levels. The final pattern observed in excitation cross sections out of metastable levels is that the magnitude of the excitation cross sections (at energies as low as 5 eV) scale very closely with the corresponding optical oscillator strengths, with only a moderate deviation for excitations with very small (or zero) oscillator strengths [6,7]. All of these patterns in experimental measurements are amply reproduced by theoretical calculations using the latest computational methods [8–11].

Within this context, we now consider excitation from the $3p^5 4s$ metastable levels of argon into the levels of the $3p^5 5p$ configuration. The $3p^5 5p \rightarrow 3p^5 4s$ emissions from the decay of $3p^5 5p$ levels occur in the blue end of the spectrum (395–470 nm) and are widely used in plasma diagnostics. Comparing $3p^5 4p$ with $3p^5 5p$ we find the same $3p^5$ core spin-orbit coupling but the perturbation by the outer electron is diminished as the latter advances from $4p$ to $5p$. This suggests the possibility that the Ar($3p^5 5p$) levels may be adequately characterized by $j_c$ with a greater preference for core preservation ($\Delta j_c = 0$) in the Ar($3p^5 4s \rightarrow 3p^5 5p$) excitations than observed in the Ar($3p^5 4s \rightarrow 3p^5 4p$) excitations. Beyond this difference, we expected the $3p^5 4s \rightarrow 3p^5 5p$ cross sections to be similar to our earlier measurements of $3p^5 4s \rightarrow 3p^5 4p$ cross sections albeit with smaller magnitudes due to the smaller $3p^5 4s$–$3p^5 5p$ oscillator strengths. While the energy dependence of the Ar($3p^5 5p$) and Ar($3p^5 4p$) excitation cross sections are indeed similar, the magnitude of the cross sections are found to deviate substantially from the expected oscillator strength scaling relation.

In Sec. II we review the experimental method and apparatus employed to measure cross sections into nine of the ten

 

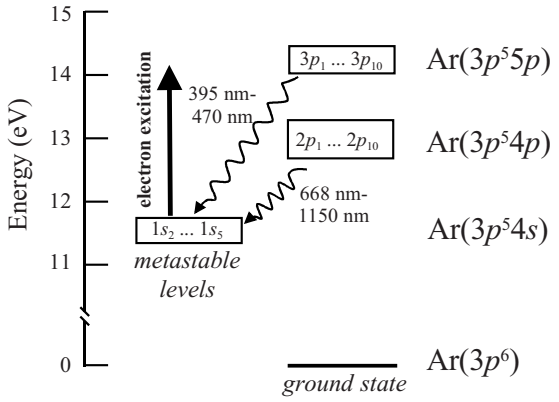


FIG. 1. Partial energy level diagram of relevant Ar energy levels. Rectangles represent groups of levels within each configuration.

$3p^5 5p$ levels from the two metastable levels of Ar. In Sec. III we present our results, followed by an analysis of these results in Sec. IV. First, however, we briefly describe in detail the atomic structure of the $3p^5 5p$ levels considered in this paper.

### B. Electronic structure and notations

The ground state of Ar is the closed shell $1s^2 2s^2 2p^6 3s^2 3p^6\ {}^1S_0$. The first excited configuration $3p^5 4s$ consists of four levels with total angular momentum $J$ values of 1, 0, 1, and 2. The two levels with $J=1$ are short lived resonance levels that decay to the $J=0$ ground state, whereas the two metastable levels with $J=0$ and $J=2$ are dipole forbidden from decaying to the ground state and thus have radiative lifetimes well in excess of 1.3 s [12]. In Paschen's notation, these four levels are labeled as $1s_2$ and $1s_4$ for the two resonance levels and $1s_3$ ($J=0$) and $1s_5$ ($J=2$) for the two metastable levels. Within the one-configuration approximation progressively higher families of excited levels are formed by elevating one of the $3p$ electrons from the $3p^6$ ground state to an excited $nl$ orbital, such as $3p^5 4p$, $3p^5 3d$, $3p^5 5s$, $3p^5 5p$,.... A total of ten levels arise from the $3p^5 4p$ configuration with $J$ values ranging from 0 to 3. In Paschen's notation these levels are labeled as $2p_1$ to $2p_{10}$ from highest to lowest energy. Likewise, the ten levels of the $3p^5 5p$ configuration are labeled as $3p_1$ to $3p_{10}$ (see Fig. 1). The only radiative decay channel open to the levels of the $3p^5 4p$ configuration are decays to the $3p^5 4s$ levels with resulting wavelengths in the 668–1150 nm range. For the levels of the $3p^5 5p$ configuration, transitions can occur to levels in three lower lying configurations: (i) $3p^5 5p \rightarrow 3p^5 4s$ with wavelengths in the range 395–470 nm, (ii) $3p^5 5p \rightarrow 3p^5 5s$ with wavelengths in the range 2.55–3.31 $\mu$m, and (iii) $3p^5 5p \rightarrow 3p^5 3d$ with wavelengths in the range 1.42–7.73 $\mu$m.

Many of the interesting features exhibited in excitation cross sections for the rare-gas sequence Ne to Xe can be expressed in terms of two angular momenta of the $np^5 n'l$ excited states, i.e., (i) $j_c$ the angular momentum of the $np^5$ core, and (ii) the total angular momentum $J$ (the sum of spin and orbital angular momentum of the $n'l$ electron and the core). For the two heaviest atoms Kr and Xe, the spin-orbit coupling within the $np^5$ core is so large that it splits the ten levels of the $np^5 n'p$ manifolds into a group of four levels ($J=0,2,1,1$) with $j_c=1/2$ and a group of six levels ($J=0,2,1,2,3,1$) with $j_c=3/2$ and a clear assignment of $J$ and $j_c$ can be made to each level. In the case of xenon, this splitting of 1.4 eV is much larger than the energy differences within each group due to the interaction between the core and the $n'l$ electron. For Ne and Ar, however, the spin-orbit splitting of the ion core is much smaller. In the case of Ar, this 0.17 eV splitting is insignificant compared to the energy differences within each $j_c$ grouping of the $3p^5 4s$ and $3p^5 4p$ manifolds leaving only $J$ as a useful label. With the extra quantum number $j_c$ in Kr and Xe, the distinction between core-preserving ($\Delta j_c=0$) and core-changing ($\Delta j_c=\pm 1$) excitation has led to many interesting features in the excitation cross sections that are not observed in the Ar($3p^5 4s \rightarrow 3p^5 4p$) and Ne($2p^5 3s \rightarrow 2p^5 3p$) series [13].

The levels of Ar($3p^5 5p$) are an interesting intermediate case between the two extremes discussed in the preceding paragraph. Whereas the spin-orbit splitting of the $3p^5$ core is all but overwhelmed by the strong coupling to the outer $4p$ electron in the $3p^5 4p$ configuration, it is much more noticeable in the levels of the $3p^5 5p$ configuration due to reduced coupling with the outer electron in the larger $5p$ orbital. This brings $j_c$ closer to being a good quantum number. Indeed, the ten levels in the $3p^5 5p$ configuration, spanning a total energy range of only 0.28 eV, do tend towards a four-six two tier structure (separated by the 0.17 eV spin-orbit splitting) as seen in Kr and Xe.

In comparison to the Paschen notation used in this paper, Racah notation more clearly indicates the ion core of the level. In this scheme a $3p^5 nl$ level is labeled $nl[K]_J$, where $K$ is the intermediate vector sum of $j_c$ and $l$, the orbital angular momentum of the outer valence electron. The total angular momentum $J$ is the vector sum of $K$ and the spin $s=1/2$ of the $nl$ electron. A prime on the $nl$ indicates a level has $j_c=1/2$ whereas levels with $j_c=3/2$ are left unprimed.

The $jK$ coupling scheme is no more than an approximation of the true intermediate coupling of the lower configurations of argon, but is widely used nonetheless. Table I is provided to aid in switching between the Racah and Paschen labeling schemes.

## II. EXPERIMENTAL METHOD

### A. Apparatus

The present work utilizes the same apparatus as in our previous Ar work [2], thus only a brief description of the apparatus follows. Metastable argon atoms are created in a hollow cathode discharge (50 mA, 3 Torr) and exit via a 1-mm-diam hole in the cathode. After exiting the discharge, the atoms are crossed by a monoenergetic electron beam. Electrons excite metastable atoms into levels of the $3p^5 5p$ manifold. Fluorescence from the decay of excited atoms is collected at right angles to the atomic beam and at a 60° angle relative to the electron beam. Narrow-band interference filters (0.3–1.5 nm FWHM) are used to isolate a par-

TABLE I. Ar energy levels in various labeling schemes. $E$ is the energy of the level relative to the ground state.

| Paschen | $J$ | $j_c$ | Racah | $E$ (eV) |
|---|---|---|---|---|
| $3p_1$ | 0 | 1/2 | $5p'\left[\frac{1}{2}\right]_0$ | 14.74 |
| $3p_2$ | 1 | 1/2 | $5p'\left[\frac{1}{2}\right]_1$ | 14.69 |
| $3p_3$ | 2 | 1/2 | $5p'\left[\frac{3}{2}\right]_2$ | 14.69 |
| $3p_4$ | 1 | 1/2 | $5p'\left[\frac{3}{2}\right]_1$ | 14.66 |
| $3p_5$ | 0 | 3/2 | $5p\left[\frac{1}{2}\right]_0$ | 14.58 |
| $3p_6$ | 2 | 3/2 | $5p\left[\frac{3}{2}\right]_2$ | 14.53 |
| $3p_7$ | 1 | 3/2 | $5p\left[\frac{3}{2}\right]_1$ | 14.52 |
| $3p_8$ | 2 | 3/2 | $5p\left[\frac{5}{2}\right]_2$ | 14.51 |
| $3p_9$ | 3 | 3/2 | $5p\left[\frac{5}{2}\right]_3$ | 14.50 |
| $3p_{10}$ | 1 | 3/2 | $5p\left[\frac{1}{2}\right]_1$ | 14.46 |
| $1s_2$ | 1 | 1/2 | $4s'\left[\frac{1}{2}\right]^o_1$ | 11.83 |
| $1s_3$ | 0 | 1/2 | $4s'\left[\frac{1}{2}\right]^o_0$ | 11.72 |
| $1s_4$ | 1 | 3/2 | $4s\left[\frac{3}{2}\right]^o_1$ | 11.62 |
| $1s_5$ | 2 | 3/2 | $4s\left[\frac{3}{2}\right]^o_2$ | 11.55 |

ticular $3p^5 5p \rightarrow 3p^5 4s$ transition of interest. Photons of the desired wavelengths are detected by an EMI 9658B (S-20 cathode) photomultiplier tube (PMT) operating in photon counting mode. Note that the 60° angle between the electron beam axis and optical axis is approximately equal to the "magic angle" of 54.7°, where the emission intensity is equal to the average intensity independent of the polarization of the radiation [14]. Thus, since the detector combination of an interference filter and PMT is relatively polarization insensitive, essentially no correction is needed for any possible polarization effects.

The thermal beam emerging from the hollow cathode contains atoms in three levels: (i) the ground state, (ii) the $1s_3$ ($J=0$) metastable level, and (iii) the $1s_5$ ($J=2$) metastable level. At electron energies below the threshold for ground state excitation (~14.5 eV), the excitation signal contains no contribution from the otherwise overwhelming number of ground state atoms emerging from the discharge ($n_{meta} \approx 3 \times 10^8$ cm$^{-3}$, $n_{gs} \approx 10^{14}$ cm$^{-3}$). The relative population of the $1s_3$ and $1s_5$ levels is measured experimentally by laser-induced fluorescence (LIF) (see Ref. [13] for further details). In our earlier measurements on excitation into the Ar($3p^5 4p$) levels, we found the ratio of the $1s_5$ to $1s_3$ number density ratio to be $5.6 \pm 1.6$ [2], which is close to the statistical weight ratio of 5. These earlier measurements, however, were conducted with a multimode Ti:sapphire laser, which complicates the analysis. In the present work, we used a single-mode Ti:sapphire laser to find a ratio of $1s_5$ to $1s_3$ of $5.0 \pm 1.1$. The small (within uncertainties) difference can be attributed to the difference in Ti:sapphire lasers used.

### B. Laser quenching

The emission signal collected is, in general, due to electron-impact excitation out of both metastable levels. In order to measure cross sections from a single metastable level in the region between exit of the hollow cathode and the electron beam, we use a laser to quench and depopulate one of the two metastable levels. To depopulate the fraction of atoms in the target initially in the $1s_5$ metastable level, we pump atoms out of the $1s_5$ level into the $J=2$ $2p_8$ level (801.5 nm). Atoms in the $2p_8$ preferentially decay to the $J=1$ $1s_2$ and $1s_4$ levels (branching fractions of 0.05 and 0.68), both of which decay to the ground level. Since the $J=2$ $2p_8$ level is dipole forbidden from decaying to the $J=0$ $1s_3$ level, the number of atoms in the target in the $1s_3$ metastable level remains unchanged.

With sufficient laser intensity and a long dwell time in the laser beam, virtually all of the $1s_5$ atoms are transferred to the ground state, leaving only metastable atoms in the $1s_3$ level in the thermal atomic beam. In contrast to the LIF measurements made with a single-mode Ti:sapphire laser, for quenching we found it desirable to use a multimode Ti:sapphire laser since the mode structure of the multimode laser better matches the Doppler-broadened profile of the atoms emerging from the discharge. We detect whether or not the $1s_5$ level is completely depopulated by observing the $2p_9 \rightarrow 1s_5$ (811.5 nm) electron excitation signal. In our previous work, we found that excitation into the $2p_9$ arises entirely due to electron-impact excitation from the $1s_5$ level [2,5]. In our measurement of electron excitation cross sections, we operate with the intensity of the laser high enough (>150 mW in a 5-mm-diam beam) that the $1s_5$ level is completely depopulated.

In addition to quenching the $1s_5$ level, we can also quench the $1s_3$ level by pumping atoms from the $1s_3$ to the $2p_4$ ($J=1$) level (794.8 nm). Atoms in the $2p_4$ level decay preferentially to the $1s_2$, $1s_3$, and $1s_5$ levels (branching fractions of 0.42, 0.56, and 0.02, respectively). The most desirable of these decay channels is to the $1s_2$ level which rapidly decays to the ground level. Atoms that decay back to the $1s_3$ level must be repumped back to the $2p_4$ level. Since the branching fraction for the $2p_4 \rightarrow 1s_3$ decay channel is rather large, quenching the $1s_3$ metastable level is less efficient than the

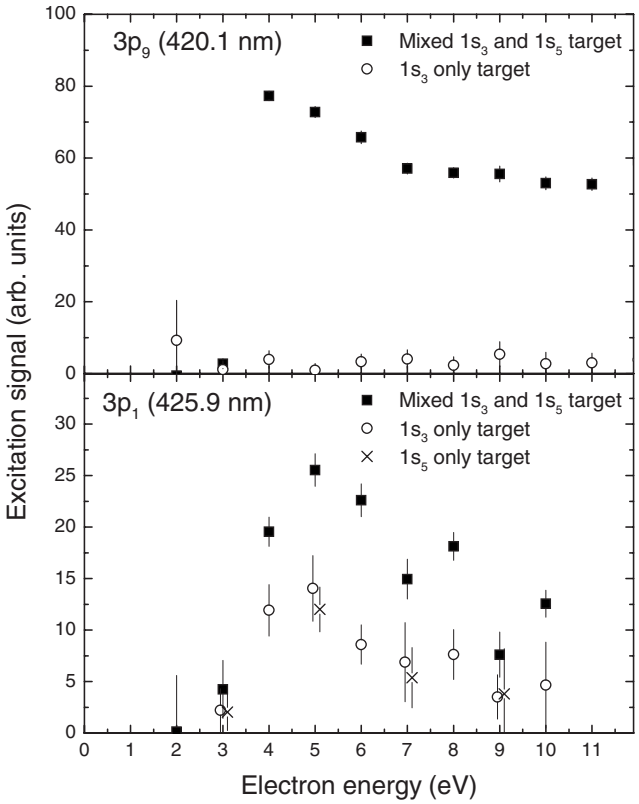


FIG. 2. Quenching results for $3p_9$ and $3p_1$ levels. In the lower graph some of the points have been offset for clarity.

$1s_5$ quenching described in the previous paragraph. Furthermore, atoms pumped into the $2p_4$ level can also decay into the $1s_5$ metastable level. However, since the number of atoms in the $1s_3$ level is a factor of 5 smaller than the $1s_5$ population in the mixed target; the small fraction of $1s_3$ atoms transferred into the $1s_5$ level does not result in a measurable increase in the population of the $1s_5$ level.

We carry out cross section measurements with three sets of targets: (i) a mixed beam containing both $1s_5$ and $1s_3$ metastable atoms, (ii) a pure $1s_3$ target obtained by quenching the $1s_5$ atoms, and (iii) a pure $1s_5$ target obtained by quenching the $1s_3$ atoms. Since (i) is essentially the sum of (ii) and (iii), taking measurements with all three possible targets provides a redundancy check of the individual measurements. Sample quenching results are shown in Fig. 2 for excitation into the $3p_9$ and $3p_1$ levels. As with the $2p_9$ results in our earlier work [5], excitation into the $3p_9$ level is almost entirely from the $1s_5$ metastable level, resulting in insignificant signal rates when the quenching laser completely depopulates the $1s_5$ level. For the $3p_1$ level, the signal contributions due to electron excitation of both metastable levels is about the same, so that quenching either the $1s_3$ or $1s_5$ metastable level reduces the mixed signal by roughly a factor of 2. While the signal rates from the two metastable levels are about equal, this does not imply that the cross sections are equal since the $1s_5$ number density in the mixed target is approximately five times larger than the $1s_3$ number density.

### C. Calibration of optical emission cross sections

The general technique used to measure $3p^5 5p$ excitation cross sections follows along the same lines as we have used previously to measure the $3p^5 4p$ excitation cross sections [2]. The emission signal $S_x$ measured at wavelength λ as a function of the incident electron energy $E$ is equal to

$$S_x(E) = C\xi_\lambda n_x Q_x(E) I_e(E), \tag{1}$$

where $Q_x(E)$ is the desired excitation cross section out of level $x$, $n_x$ is the number density of target atoms in initial level $x$, $I_e(E)$ is the electron beam current, $\xi_\lambda$ is the efficiency of the optical system at the observed wavelength, and $C$ is a constant that includes numerous conversion factors, the solid angle of the viewing region, and overlap integrals of the electron beam, atomic beam, and viewing region. As compared to working with ground state static gas targets, it is difficult to directly measure many of the quantities in Eq. (1) including $n_x$, $C$, and $\xi_\lambda$. Since the constant $C$ is especially difficult to measure, we instead measure four separate signals to extract the $3p_x$ metastable cross section: (i) the metastable excitation signal for the $3p_x$ level of interest $S_m^{3p_x}$ measured on a transition of wavelength λ; (ii) the ground state excitation signal at the same wavelength $S_{gs}^{3p_x}$; (iii) the metastable excitation signal for the $2p_9$ level measured at $\lambda' = 811.5$ nm, $S_m^{2p_9}$; and (iv) the ground state excitation signal $S_{gs}^{2p_9}$. The ratio of the signal rate (i) and (ii) removes the dependence on $C$ and $\xi_\lambda$, but this ratio is proportional to $(n_m/n_0)$, where $n_m$ is the metastable target density and $n_0$ is the ground state target density. To remove the dependence on the difficult to measure metastable density, we divide the ratio of (i) to (ii) by the ratio of (iii) to (iv), which cancels out the $(n_m/n_0)$ terms, leaving

$$Q_m^{3p_x;\lambda}(E) = \frac{S_m^{3p_x}(E)}{S_m^{2p_9}(E)} \frac{S_{gs}^{2p_9}(E')}{S_{gs}^{3p_x}(E')} \frac{Q_m^{2p_9;\lambda'}(E)}{Q_{gs}^{2p_9;\lambda'}(E')} Q_{gs}^{3p_x;\lambda}(E'), \tag{2}$$

where $E$ is the calibration energy used for the metastable measurements (8 eV), and $E'$ is the energy used for the ground state excitation measurements (20 eV). Note that λ in the superscript to $Q_m^{3p_x;\lambda}$ is meant to indicate that the cross section is technically an *optical emission* cross section, since the measurement is only proportional to the cross section that results in the emission of a photon at the observed wavelength. Also note that for measurements taken with a mixed $1s_3$ and $1s_5$ metastable target, the metastable cross sections in Eq. (2) should be replaced with a sum over the cross sections out of each metastable level weighted by the number density of atoms in each of the metastable levels, i.e., $Q_m \Rightarrow \Sigma w_m Q_m$. Since the $2p_9$ level is solely populated by excitation from the $1s_5$ metastable level, this correction only needs to be applied to the $3p_x$ excitation cross sections on the left-hand side of Eq. (2). In that case, $w_{1s_5} = 1$ for excitation from the $1s_5$ metastable level, and $w_{1s_3} = 1/(5.0 \pm 1.1)$ for the $1s_3$ metastable level.

Cross sections for excitation into the $2p_9$ and $3p_x$ levels from the *ground state* are widely available in the literature [1,15–18]. To minimize uncertainties introduced by certain possible systematic effects [1], we have used the optical

TABLE II. Quantities involved in determining metastable excitation cross sections into Ar $3p^5 5p$ levels. The optical emission cross section at 8 eV for excitation from a mixed target of metastable atoms is measured in relation to the peak optical emission cross section from the ground state (at 20 eV). This optical emission cross section is converted into an apparent cross section by dividing by the branching fraction $\Gamma_\lambda$ of the observed transition.

| Level | λ (nm) | $Q_{gs}^{Opt}$ [a] ($10^{-20}$ cm$^2$) | $\Sigma w_m Q_m^{Opt}$ ($10^{-18}$ cm$^2$) | $\Gamma_\lambda$ [b] | $\Sigma w_m Q_m^{App}$ ($10^{-16}$ cm$^2$) |
|---|---|---|---|---|---|
| $3p_1$ | 425.9 | 32 | 0.49 | 0.341 | 0.014 |
| $3p_2$ | 394.9 | 5.4[c] | 1.10 | 0.057 | 0.19 |
| $3p_4$ | 434.5 | 4.3 | 0.96 | 0.043 | 0.22 |
| $3p_5$ | 451.1 | 11 | 0.44 | 0.091 | 0.048 |
| $3p_6$ | 415.9 | 23 | 8.9 | 0.145 | 0.62 |
| $3p_7$ | 427.2 | 18 | 1.5 | 0.095 | 0.16 |
| $3p_8$ | 430.0 | 17[d] | 2.8[e] | 0.050 | 0.56 |
| $3p_9$ | 420.1 | 49[f] | 10.3[g] | 0.109 | 0.95 |
| $3p_{10}$ | 470.2 | 2.8 | 0.94 | 0.019 | 0.49 |

[a]Reference [18].
[b]Reference [24].
[c]Effective value, includes a 39% contribution from 394.8 nm emission line.
[d]Effective value, includes a 12% contribution from 427.2 nm emission line.
[e]Corrected for 427.2 nm metastable contribution (−5%).
[f]Effective value, includes a 33% contribution from 419.8 nm emission line.
[g]Corrected for 419.8 nm metastable contribution (−6%).

emission cross sections from Ref. [18]. The metastable $1s_5 \rightarrow 2p_9$ excitation cross section was measured absolutely in our previous work using a fast beam target [2]. The measured value of $(24 \pm 8) \times 10^{-16}$ cm$^2$ is in excellent agreement with *R*-matrix theoretical value of $25 \times 10^{-16}$ cm$^2$ as calculated in Ref. [11].

The optical emission cross sections derived from Eq. (2) are equal to the total apparent cross section into the level $3p_x$ times the branching fraction of the observed $3p_x \rightarrow 1s_y$ emission line. In principle, the total (apparent) cross section into the $3p_x$ level could be determined by summing up the optical emission cross sections for all transitions out of the $3p_x$ level. However, this is exceedingly difficult due to the number of measurements required and the infrared wavelengths of the $3p^5 5p \rightarrow 3p^5 5s, 3p^5 3d$ transitions. Assuming the branching fraction for $3p_x \rightarrow 1s_y$ transition is known, the $3p_x$ apparent cross section is simply,

$$Q_m^{3p_x}(E) = \Gamma_\lambda^{-1} Q_m^{3p_x;\lambda}(E), \tag{3}$$

where $\Gamma_\lambda$ is the branching fraction for the observed transition. A variation of this method was used in our previous measurements of excitation cross sections into the $3p_x$ levels from the ground state [15], where the branching fractions were derived from transition probability measurements of the $3p^5 4s$–$3p^5 5p$ transition array [19] and lifetime measurements of the $3p^5 5p$ levels [20–23]. Relatively large uncertainties in the lifetime measurements contributed considerably to the total uncertainties in the derived apparent cross sections. Recent *B*-spline calculations of the required transition probabilities [24] agree reasonably well with the values derived from experimental measurements (−10 to +30%), but have a much lower estimated uncertainty (effectively ≤5% versus ~15%).

## III. RESULTS

The absolute calibration results of the mixed target measurements are presented in Table II. For three of the measurements, narrow-band interference filters were unable to completely resolve the desired transition (at $\lambda_1$) from nearby contaminating lines (at $\lambda_2$). In these cases the effective ground state optical emission cross section $Q_{gs}^{3p_x;\lambda_1}$ was replaced by the sum of the desired optical emission cross section plus the optical emission cross section of the contaminating line weighted by the relative filter transmission at $\lambda_2$. In addition to contributing to the observed ground state excitation signal, the contaminating line also contributes a small amount to the metastable excitation signal. For example, the $3p_9$ excitation signal at 420.1 nm (using a filter with a FWHM of 0.3 nm) includes a small contribution from the 419.8 nm emission line due to excitation into the $3p_5$ level. For excitation from the ground state, the 419.8 nm and 420.1 nm optical emission cross sections are similar in magnitude, leading to a substantial correction to the effective ground state cross section used. For excitation from the metastable levels, however, the cross section into the $3p_5$ level is substantially smaller than the cross section into the $3p_9$ level, leading to a much smaller addition to the (419.8 +420.1 nm) mixed signal. The exact correction is found by measuring the $3p_5$ cross section with the 451.1 nm emission line, and multiplying by the ratio of the 419.8 nm branching fraction of the $3p_5$ level to the 451.1 nm branching fraction. No results were obtained for the $J=2$ $3p_3$ level due to the

TABLE III. Apparent cross section values from $J=0$ $1s_3$ and $J=2$ $1s_5$ metastable levels. Quoted uncertainties at 8 eV are a combination of the statistical uncertainties and the ±40% systematic uncertainties in the overall magnitudes. Uncertainties for cross sections out of the $1s_3$ metastable levels also include a contribution from determining the ratio of the $1s_3$:$1s_5$ number densities.

| | Cross section ($10^{-16}$ cm$^2$) | | | | |
|---|---|---|---|---|---|
| Excitation | 4 eV | 5 eV | 6 eV | 8 eV | 10 eV |
| $1s_3 \rightarrow 3p_1$ ($J=0$) | 0.043 | 0.062 | 0.052 | 0.041±0.018 | 0.027 |
| $1s_3 \rightarrow 3p_2$ ($J=1$) | 0.77 | 0.97 | 0.83 | 0.86±0.37 | 0.68 |
| $1s_3 \rightarrow 3p_4$ ($J=1$) | 1.00 | 0.97 | 0.94 | 0.95±0.39 | 0.87 |
| $1s_3 \rightarrow 3p_7$ ($J=1$) | 0.20 | 0.22 | 0.12 | 0.15±0.09 | |
| $1s_3 \rightarrow 3p_{10}$ ($J=1$) | 0.31 | 0.39 | 0.35 | 0.27±0.24 | |
| $1s_5 \rightarrow 3p_1$ ($J=0$) | | 0.020 | | 0.008±0.006 | |
| $1s_5 \rightarrow 3p_2$ ($J=1$) | 0.070 | 0.069 | 0.042 | 0.023±0.015 | |
| $1s_5 \rightarrow 3p_4$ ($J=1$) | | | | 0.047±0.029 | |
| $1s_5 \rightarrow 3p_5$ ($J=0$) | 0.136 | 0.097 | 0.066 | 0.048±0.020 | 0.047 |
| $1s_5 \rightarrow 3p_6$ ($J=2$) | 0.85 | 0.81 | 0.70 | 0.66±0.26 | 0.53 |
| $1s_5 \rightarrow 3p_7$ ($J=1$) | 0.31 | 0.25 | 0.21 | 0.15±0.06 | 0.12 |
| $1s_5 \rightarrow 3p_8$ ($J=2$) | 0.83 | 0.75 | 0.71 | 0.56±0.23 | 0.51 |
| $1s_5 \rightarrow 3p_9$ ($J=3$) | 1.23 | 1.19 | 1.10 | 0.95±0.39 | 0.89 |
| $1s_5 \rightarrow 3p_{10}$ ($J=1$) | 0.30 | 0.47 | 0.45 | 0.48±0.20 | 0.47 |

difficulty in finding a suitable transition that could be resolved from neighboring lines.

The $1s_3+1s_5$ mixed target results of Table II can be further separated into individual cross sections for each metastable level by the laser quenching method described in Sec. II B. In some cases such as the $J=2$ $3p_6$ level, essentially all of the mixed excitation signal arises from the $1s_5$ level, so that $Q^{App}(1s_5 \rightarrow 3p_6)=\Sigma w_m Q_m$. For the $J=0$ $3p_1$ excitation signal illustrated in Fig. 2, approximately half of the mixed signal arises from excitation of the $1s_5$ contribution and half from the $1s_3$ contribution. Taking into account the different $w_m$ weighting factors for the two levels, the mixed $\Sigma w_m Q_m$ value of $0.014 \times 10^{-16}$ cm$^2$ is apportioned into values of $Q^{App}(1s_5 \rightarrow 3p_1)=0.008 \times 10^{-16}$ cm$^2$ and $Q^{App}(1s_3 \rightarrow 3p_1)=0.041 \times 10^{-16}$ cm$^2$. For the $3p_8$ and $3p_9$ levels the measured optical emission cross sections at each incident electron energy were corrected for the small contributions from neighboring lines.

Apparent cross section values at selected energies are listed in Table III. Excitation functions (cross section as a function of incident electron energy) for apparent cross sections out of the $1s_5$ ($J=2$) metastable level are displayed in Fig. 3, while apparent cross sections out of the $1s_3$ ($J=0$) metastable level are displayed in Fig. 4. Error bars in the figure reflect only the relative statistical uncertainty, and do not include the systematic uncertainty arising from placing the values on an absolute scale. The total systematic uncertainty is estimated to be ±40%, with most of this total arising from ±35% uncertainty in the $1s_5 \rightarrow 2p_9$ cross section used for calibration [2]. Since this 35% uncertainty in the absolute magnitude is common to all the cross sections, the relative uncertainty between any two levels is typically not much larger than the statistical uncertainties. Thus the error bars in Figs. 3 and 4 depict the uncertainty of the relative values and energy dependence of the cross sections which are not affected by the uncertainty of the absolute calibration. While the excitation cross sections from the $1s_3$ and $1s_5$ levels into the $3p_7$ level are of similar size (both $0.15 \times 10^{-16}$ cm$^2$ at 8 eV), the signal rates from the two metastable levels differ substantially due to the 5:1 $1s_5$:$1s_3$ ratio in the mixed target. This is also the case for excitation from the $1s_3$ and $1s_5$ levels into the $3p_{10}$ level. The large statistical error bars on the $1s_3 \rightarrow 3p_7$ and $1s_3 \rightarrow 3p_{10}$ cross sections arise from the difficulty in experimentally measuring the small core-changing $1s_3 \rightarrow 3p_x$ signals. In principle, this statistical error could be decreased with additional data; however, the time required to reduce the uncertainties for these two levels to $\leqslant$15% would be impracticably long considering that laser quenching must be used to separate $1s_3$ and $1s_5$ contributions.

The measured apparent cross sections are the sum of the direct excitation cross section plus the cascade contribution from excitation into higher levels followed by radiative decays into the level of interest. Since we cannot measure the infrared $3p^5 6s \rightarrow 3p^5 5p$ or $3p^5 4d \rightarrow 3p^5 5p$ cascades, the reported cross sections include an unknown cascade contribution. Estimates based on Born calculations suggest that metastable excitation cross sections into the $3p^5 4d$ levels are, on average, about a factor of four smaller than the cross sections into the $3p^5 5p$ levels [25]. Since the $3p^5 4d \rightarrow 3p^5 5p$ branching fractions are much more favorable than the $3p^5 4d \rightarrow 3p^5 4p$ fractions, virtually all of the $3p^5 4d$ contribution is included in our reported $3p^5 5p$ apparent cross sections. Hence, large (>25%) cascade contributions are likely for most of the results, particularly for levels with very small direct cross sections (i.e., the $3p_1$ and $3p_5$ levels).

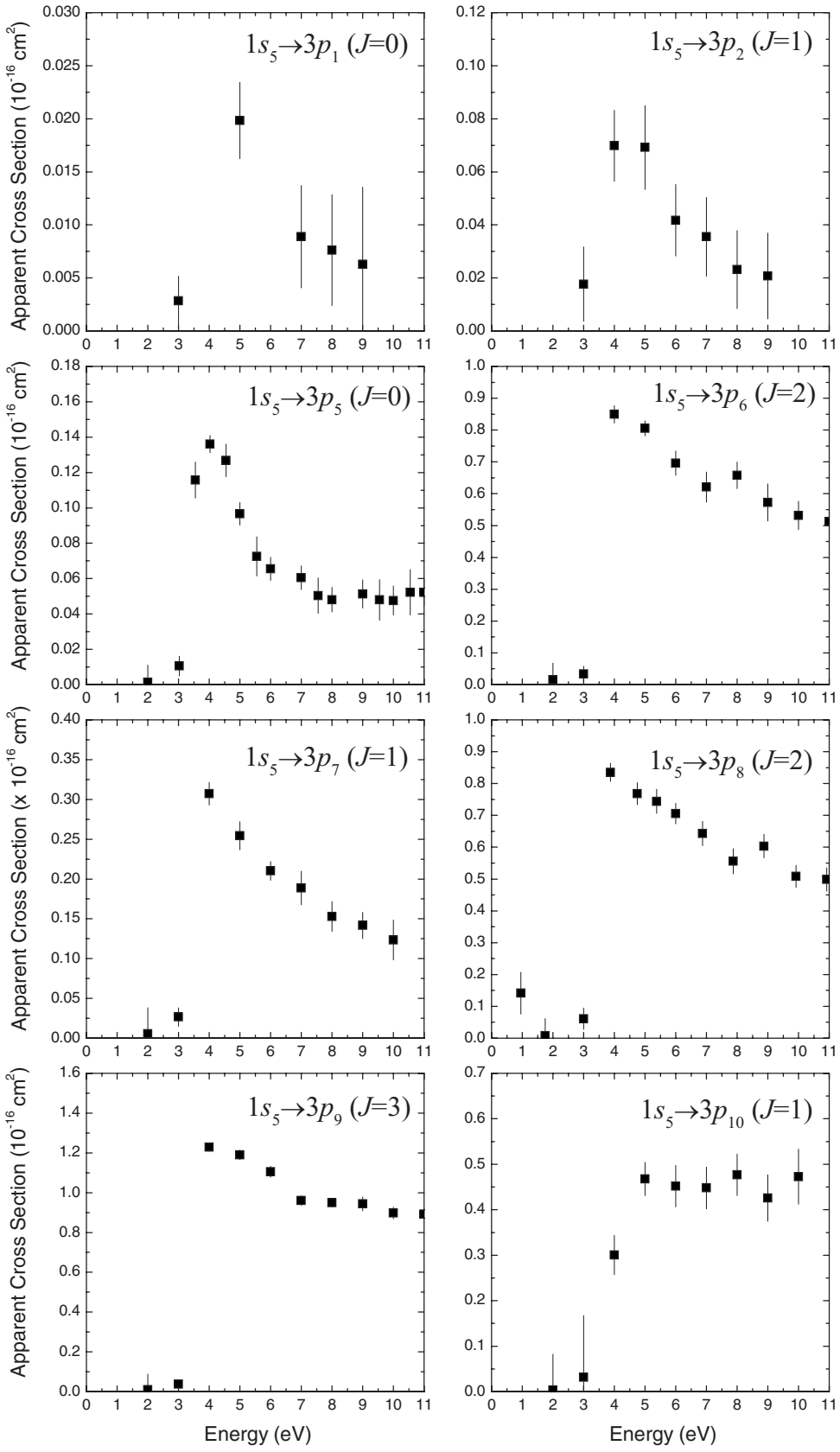


FIG. 3. Apparent cross sections for excitation into $3p^5 5p$ levels from the $J=2$ $1s_5$ metastable level. Error bars are statistical only and do not include the absolute calibration uncertainty of ±40%, but they reflect the uncertainty of the relative values and energy dependence of the cross sections.

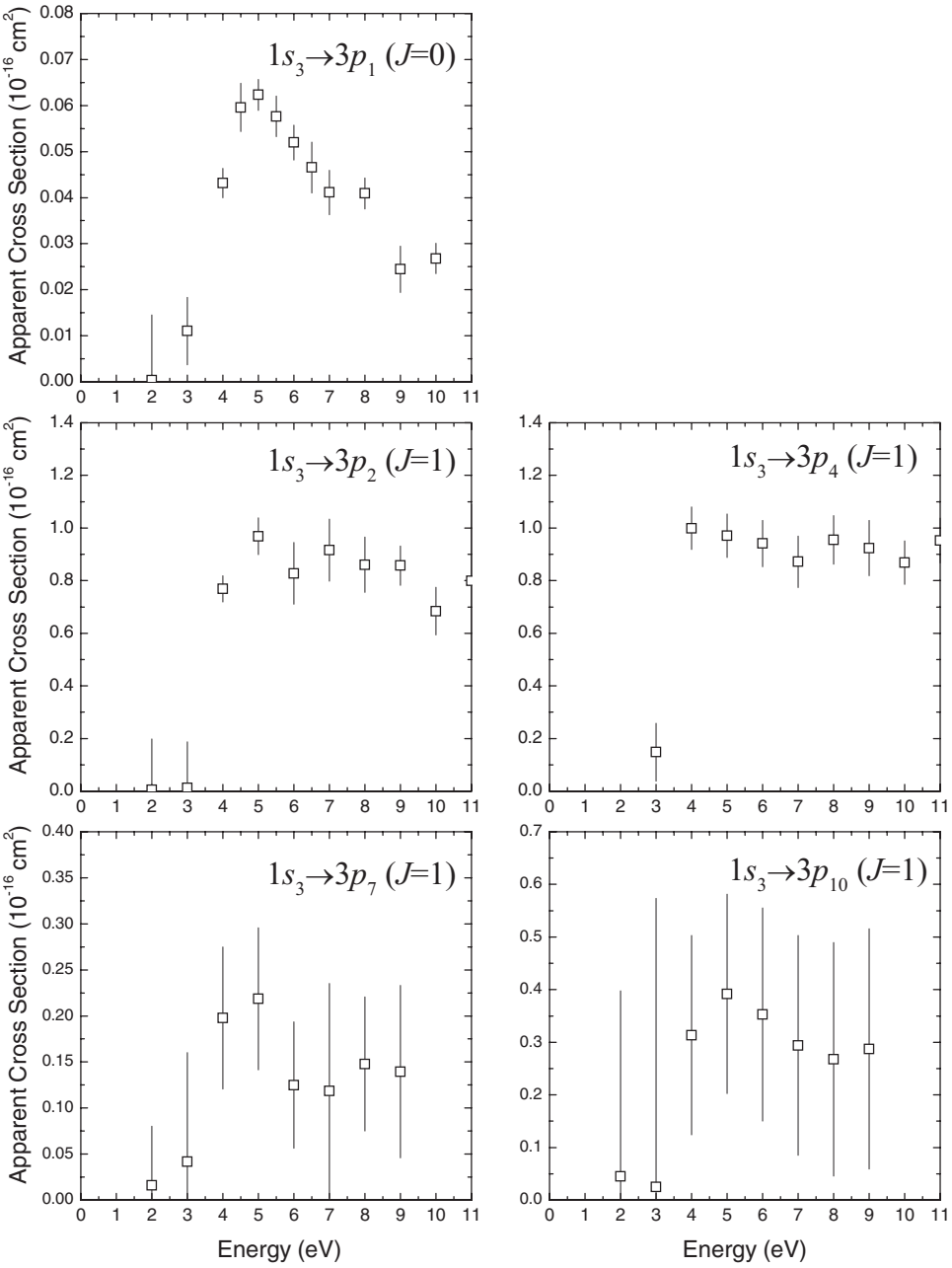


FIG. 4. Apparent cross sections for excitation into $3p^5 5p$ levels from the $J=0$ $1s_3$ metastable level. Error bars are statistical only and do not include the absolute calibration uncertainty of ±40%, but they reflect the uncertainty of the relative values and energy dependence of the cross sections.

## IV. DISCUSSION

### A. Energy dependence

Our previous measurements of the excitation cross sections from the Ar metastable levels into levels of $3p^5 4p$ configuration have revealed two general classes of excitation function shapes [2,5]. For dipole-allowed processes ($\Delta J = \pm 1, 0$ with $J=0 \not\rightarrow 0$), the cross section as a function of electron energy is relatively flat at low energies, decreasing slowly with increasing electron energy, whereas the excitation functions of dipole-forbidden excitation processes have the shape of a sharp peak, decreasing to less than a quarter of the peak value at only 10 eV. For excitation from the $J=2$ $1s_5$ metastable level, excitation into all of the $3p^5 4p$ levels are dipole allowed with the exception of the two $J=0$ levels ($2p_1$ and $2p_5$), whereas excitation from the $J=0$ $1s_3$ metastable level is only dipole allowed into the $J=1$ levels. In addition to the Ar($3p^5 4p$) excitation cross sections, the distinction between these two classes are also present in measurements for excitation of metastable Ne [26], Kr [13], and Xe [7]. For a number of the weaker, dipole-allowed excitation processes in Kr and Xe (with $i \rightarrow j$ optical oscillator strengths, $f_{ij} \lesssim 0.1$), however, the excitation functions had an intermediate shape that was dependent on the value of $f_{ij}$, approaching the sharply peaked shape of the dipole-forbidden process for $f_{ij} \lesssim 0.01$ [7].

The present Ar($3p^5 5p$) metastable excitation cross section shapes illustrated in Figs. 3 and 4 follow the general twofold dipole-allowed (dipole-forbidden) classification scheme. With the exception of the two $J=0$ levels ($3p_1$ and $3p_5$), the excitation functions are relatively broad. In contrast, the excitation functions for the dipole-forbidden processes $1s_5$

TABLE IV. Comparison of cross section magnitudes at 8 eV. The Born-Bethe values have been scaled to match the experimental $1s_5 \rightarrow 2p_9$ value [2].

| Process | $E_{ij}$ (eV) | $f_{ij}$ (Ref. [24]) | Cross section ($10^{-16}$ cm$^2$) Scaled $Q_{ij}^{BB}$ | This expt. (8 eV) |
|---|---|---|---|---|
| $1s_3 \rightarrow 3p_2$ | 2.97 | 0.0051 | 0.12 | 0.86±0.37 |
| $1s_3 \rightarrow 3p_4$ | 2.94 | 0.0041 | 0.10 | 0.95±0.39 |
| $1s_3 \rightarrow 3p_7$ | 2.80 | $9.8\times10^{-5}$ | 0.003 | 0.15±0.09 |
| $1s_3 \rightarrow 3p_{10}$ | 2.74 | 0.00087 | 0.022 | 0.27±0.24 |
| $1s_5 \rightarrow 3p_2$ | 3.14 | 0.00071 | 0.016 | 0.02±0.01 |
| $1s_5 \rightarrow 3p_4$ | 3.11 | $2.5\times10^{-7}$ | $5.8\times10^{-6}$ | 0.05±0.03 |
| $1s_5 \rightarrow 3p_6$ | 2.98 | 0.0039 | 0.094 | 0.66±0.26 |
| $1s_5 \rightarrow 3p_7$ | 2.97 | 0.00046 | 0.011 | 0.15±0.06 |
| $1s_5 \rightarrow 3p_8$ | 2.96 | 0.00081 | 0.020 | 0.56±0.23 |
| $1s_5 \rightarrow 3p_9$ | 2.95 | 0.0034 | 0.083 | 0.95±0.39 |
| $1s_5 \rightarrow 3p_{10}$ | 2.91 | 0.00019 | 0.0047 | 0.48±0.20 |

$\rightarrow 3p_1$, $3p_5$ and $1s_3 \rightarrow 3p_1$ are all sharply peaked. Nonetheless, the dipole-allowed Ar($3p^5 5p$) cross sections do have a larger decrease from the peak to 10 eV than do the Ar($3p^5 4p$) cross sections [2]. Indeed, considering that all of the optical oscillator strengths of the Ar($3p^5 5p$) dipole-allowed processes are less than 0.005, it is interesting that they are not more noticeably peaked (cf. Sec. IV B). There is some difference in shape, however, between the dipole-allowed excitation functions with the largest and smallest cross sections, i.e., flatter for the large $1s_3 \rightarrow 3p_2$ cross section, more peaky for the small $1s_5 \rightarrow 3p_2$ cross section.

For the heavier rare gases (i.e., Kr, Xe), differences in the shape and magnitude of the excitation cross sections were also found to be correlated with changes in the core angular momentum $j_c$ [13]. Excitation cross sections for core-changing processes (i.e., $1s_5 \rightarrow 3p_1 - 3p_4$, $1s_3 \rightarrow 3p_5 - 3p_{10}$ in the present case) are smaller in magnitude and more sharply peaked in energy. This core-preserving, core-changing dichotomy does not appear to be as relevant for either the Ar($3p^5 4p$) or Ar($3p^5 5p$) excitation cross sections. The best examples are found among excitation cross sections into the $J=1$ $3p^5 5p$ levels which are dipole allowed from both metastable levels. While the core-changing $1s_5 \rightarrow 3p_2$, $3p_4$ cross sections are indeed smaller than the core-preserving $1s_3 \rightarrow 3p_2$, $3p_4$ cross sections, the cross sections into the $3p_7$ and $3p_{10}$ levels have similar size cross sections for both core-changing and core-preserving processes. Furthermore, the shapes of the excitation functions are generally not so distinct between the core-preserving and core-changing categories.

### B. Relation of cross section to optical oscillator strength

Perhaps the largest difference observed between excitation from the metastable levels into the Ar($3p^5 4p$) and Ar($3p^5 5p$) levels is that the magnitude of the Ar($3p^5 5p$) cross sections fail to scale with optical oscillator strengths. Indeed, the magnitude of the metastable excitation cross sections into the Ne($2p^5 3p$), Ar($3p^5 4p$), Kr($4p^5 5p$), and Xe($5p^5 6p$) levels are all proportional to the corresponding optical oscillator strengths out of the $1s_3$ and $1s_5$ levels. The breakdown of this scaling relationship for the present experimental results is best illustrated by examining the sizes of the $1s_5 \rightarrow 3p_6$ and $1s_5 \rightarrow 3p_9$ cross sections. The $1s_5$-$3p_6$ oscillator strength value of 0.0039 is slightly larger than the $1s_5$-$3p_9$ value of 0.0034 [24], but the $1s_5 \rightarrow 3p_6$ cross section value of $0.66\times10^{-16}$ cm$^2$ at 8 eV is almost a factor of two *smaller* than the $1s_5 \rightarrow 3p_9$ cross section value of $0.95\times10^{-16}$ cm$^2$. Furthermore, the $1s_5 \rightarrow 3p_9$ cross section is only a factor of 25 smaller than the $1s_5 \rightarrow 2p_9$ cross section, whereas the $f_{ij}/E_{ij}$ values for the two processes differ by approximately a factor of 250. Additional values are listed in Table IV.

While the proportionality between excitation cross section magnitudes and optical oscillator strengths is supported by the latest theoretical calculations (i.e., Ref. [8]), it is customary to illustrate this connection with the simpler Born-Bethe approximation. Within this approximation, the $i \rightarrow j$ excitation cross section $Q_{ij}$ as a function of electron energy $E$ is

$$Q_{ij}^{BB}(E) \simeq 4\pi a_0^2 f_{ij} \frac{R^2}{EE_{ij}} \ln E, \tag{4}$$

where $a_0$ is the Bohr radius, $R$ is the Rydberg energy, $E_{ij}$ is the energy difference between the two energy levels, and $f_{ij}$ is the oscillator strength of the $i \rightarrow j$ transition. Since this expression neglects higher order $E^{-n}$ terms, it is only expected to be valid at high energies. Nonetheless, even at very low energies (within a few eV of the excitation threshold) the relative $1s_y \rightarrow 2p_x$ excitation cross sections for all the rare gases is by and large still nearly proportional to the optical oscillator strength even though the energy dependence no longer bears any resemblance to the $E^{-1} \ln E$ form [4]. This observed relationship at low energies, though not expected to be valid from the standard high-energy Born-Bethe analysis, is especially valuable for estimating cross sections within the $1s_y \rightarrow 2p_x$ array. Thus it is disappointing that a similarly useful correlation does not hold for the $1s_y \rightarrow 3p_x$ excitation series.

Note, however, the oscillator strength scaling applies to direct excitation cross sections, whereas the measured apparent cross sections are equal to the direct excitation cross section plus an unknown cascade component due to excitation into higher levels. For excitation into $np^5(n+1)p$ levels, where the cross sections do scale with oscillator strengths, the cascade contributions to the apparent cross sections are small (i.e., $<10\%$) [2]. Since cascades into the Ar($3p^5 5p$) levels may be larger (i.e., $\simeq 25\%$), some departures are to be expected when comparing apparent cross sections to the oscillator strength scaling. Even a 25% cascade contribution, however, is insufficient to explain the differences between levels within the $3p^5 5p$ manifold (i.e., the $1s_5 \rightarrow 3p_9$ cross section being much larger than the $1s_5 \rightarrow 3p_6$ cross section) or between the levels of the $3p^5 4p$ and $3p^5 5p$ manifolds.

While the Born-Bethe approximation as expressed in Eq. (4) does a poor job on the $3p^5 5p$ cross sections, only a slightly more complicated plane-wave Born calculation does

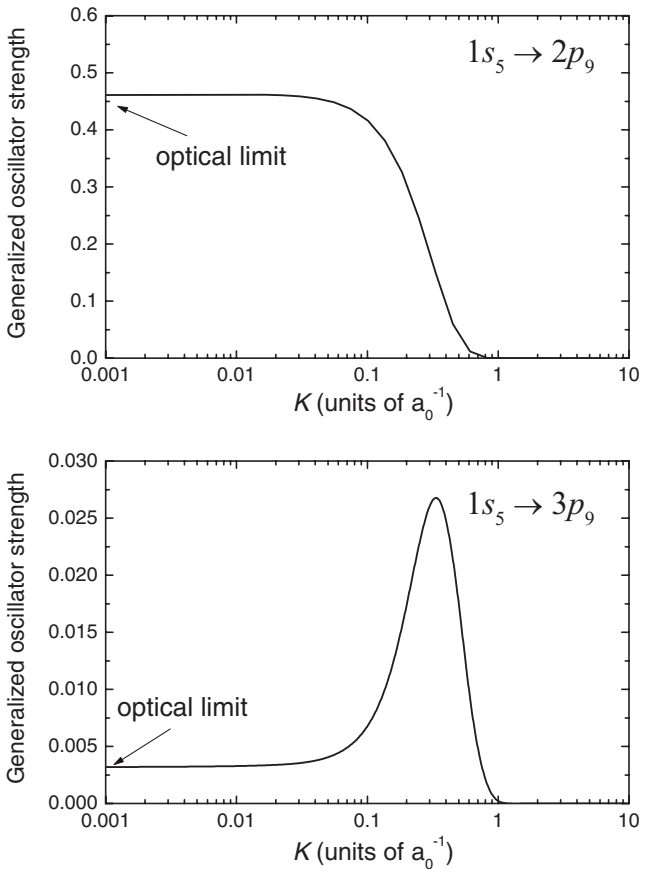


FIG. 5. Generalized oscillator strengths for the $1s_5 \rightarrow 2p_9$ and $1s_5 \rightarrow 3p_9$ excitation processes.

a much better job. For example, the configuration-averaged Born approximation values of Hyman correctly reproduces the relative size of the $3p^5 4s \rightarrow 3p^5 5p$ cross sections in comparison to the $3p^5 4s \rightarrow 3p^5 4p$ cross sections [25]. Hence, some appreciation of the underlying reasons for the scaling relationship, as well as the lack of it, can be obtained by understanding the differences between the Born and Born-Bethe approximations as it relates to the $4s \rightarrow 4p$ and $4s \rightarrow 5p$ excitation processes.

The electron-excitation cross section (in units of $\pi a_0^2$) from level $i$ to $j$ can be expressed in the Born approximation as

$$Q_{ij}^{PWB}(E) = \frac{8}{EE_{ij}} \int_{K_{min}}^{K_{max}} g_i f_{ij}(K) d(\ln K), \tag{5}$$

where $g_i$ is the statistical weight of the initial level $i$, $K$ is the momentum transfer of the scattered electron of incident electron energy $E$ (measured in rydbergs) and $f_{ij}(K)$ is the generalized oscillator strength [27,28]. The energy dependence of the cross section enters via the limits of the $K$ integration which are functions of the incident electron energy $E$ and the excitation threshold energy $E_{ij}$. In the limit of $K \rightarrow 0$ the generalized oscillator strength equals the optical oscillator strength. In Fig. 5 we illustrate how the generalized oscillator strengths vary with $K$ for two representative examples, namely, the $1s_5 \rightarrow 2p_9$ and $1s_5 \rightarrow 3p_9$ excitation processes. Here the horizontal axis is logarithmic so that the area under the curves between $K_{min}$ and $K_{max}$ gives the cross section in accordance with Eq. (5).

Consider first the $1s_y \rightarrow 2p_x$ series. The general shape of the $1s_5 \rightarrow 2p_9$ curve in Fig. 5 is, in fact, representative of the dipole-allowed $1s_y \rightarrow 2p_x$ generalized oscillator strengths, only the overall magnitude (i.e., the value at $K=0$) differs between different excitation processes. From the shape of the $1s_5 \rightarrow 2p_9$, it is clear why the simple Born-Bethe approximation works as well as it does. For low incident electron energies, the major part of the integrand covers only a small $K$ range around $0.3a_0^{-1}$. At a high electron energy $K_{max}$ far exceeds the value of $0.7a_0^{-1}$ beyond which the generalized oscillator strength becomes negligible so that $K_{max}$ can be replaced by a constant cutoff value $K_{cut}$. Since $K_{min}$ varies with electron energy like $E^{-1/2}$, as $E$ becomes larger the lower limit of the Born integral shifts drastically to the left in Fig. 5 on account of the logarithmic scale. The integral is then dominated by the area under the plateau region proportional to $f_{ij}(K=0)\ln E$, hence the familiar Born-Bethe formula of Eq. (5). The above analysis obviously fails at low energies because, for example, at 5 eV we find $K_{max}=1.2a_0^{-1}$ and $K_{min}=0.1a_0^{-1}$ for the $1s_5 \rightarrow 2p_9$ excitation. Hence, the cross section comes entirely from the descending part of the $f_{ij}(K)$ curve, thus no $E^{-1} \ln E$ dependence can be expected. Nonetheless, because the generalized oscillator strength curves for all the $1s_y \rightarrow 2p_x$ excitations have the same general shape differing only in the asymptotic value at $K=0$, the Born integrals for a given energy vary primarily according to a scaling factor represented by the $K=0$ optical oscillator strength. Thus even at near-threshold energies the popular Born-Bethe formula as stated in Eq. (5) amazingly appears to be applicable to the $1s_y \rightarrow 2p_x$ group as far as the scaling relation with respect to the optical oscillator strength is concerned, although the $E^{-1} \ln E$ dependence is completely invalidated.

In contrast to the simple shape of the $1s_5 \rightarrow 2p_9$ generalized oscillator strength in Fig. 5, that of the $1s_5 \rightarrow 3p_9$ is far more complex. As with the $1s_5 \rightarrow 2p_9$ curve, $f_{ij}(K)$ approaches the optical oscillator strength as $K \rightarrow 0$, but in addition, there is a large peak near $0.3a_0^{-1}$. At low to moderate electron energies the area of this peak in the Born integral dominates the contribution from the $f_{ij}(K=0)\ln E$ portion in the plateau region. Thus, the presence of the peak is the reason why the plane-wave-Born cross section, which includes the area of the peak, better approximates the $1s_5 \rightarrow 3p_9$ excitation cross section than the Born-Bethe value which only includes the much smaller $f_{ij}(K=0)\ln E$ contribution. Furthermore, if the height of the auxiliary peak is not closely related to the $K=0$ optical oscillator strength limit for different $1s_y \rightarrow 3p_x$ processes, then there is no reason to expect the excitation cross sections to be proportional to the optical oscillator strengths even at moderately high electron energies.

Having traced the nonscaling of the $1s_y \rightarrow 3p_x$ to the presence of the peak in the generalized oscillator strength, we now address the reason why the additional peak is present in the $3p^5 4s$–$3p^5 5p$ generalized oscillator strengths but absent in the $3p^5 4s$–$3p^5 4p$ case. Neglecting all of the angular momentum coupling algebra, the dependence of the generalized

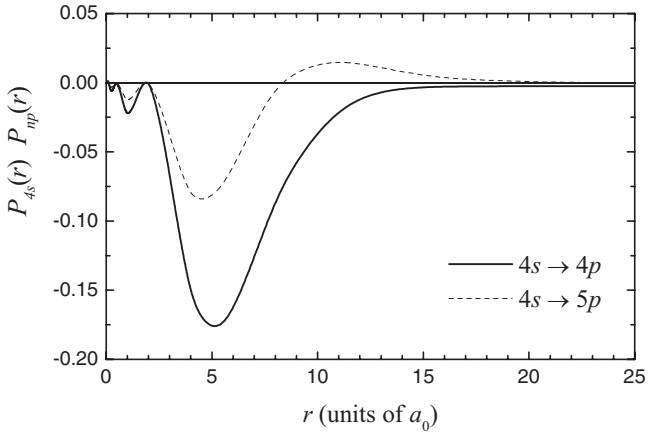


FIG. 6. Product of the $P_{4s}(r)P_{4p}(r)$ and $P_{4s}(r)P_{5p}(r)$ radial wave functions.

oscillator strength on the radial wave functions of the jumping $4s \rightarrow np$ electron can be decomposed into a sum of integrals with a weighting factor in the form of

$$f_{ij}(K) \sim \sum_t a_t \left( \int_0^\infty P_{4s}(r) j_t(Kr) P_{np}(r) dr \right)^2, \qquad (6)$$

where $P_{4s}(r)$ and $P_{np}(r)$ are the radial wave functions (multiplied by $r$), and $j_t(Kr)$ is a spherical Bessel function of order $t$ [27]. The exact terms included in the sum over $t$ are governed by angular momentum coupling selection rules, but for illustrative purposes we simply note that the $j_t(Kr)$ function in the integrand acts as a damped oscillator. Without this term, the product of the $P_{4s}(r)P_{4p}(r)$ and $P_{4s}(r)P_{5p}(r)$ radial wave functions are shown in Fig. 6. For the $3p^5 4s \rightarrow 3p^5 4p$ excitation process, the product of $P_{4s}(r)$ and $P_{4p}(r)$ has the same sign for all $r$. Hence, the introduction of the $j_t(Kr)$ oscillatory can do nothing but reduce the product of $P_{4s}(r)j_t(Kr)P_{4p}(r)$ for all values of $K$. In contrast, for $3p^5 4s \rightarrow 3p^5 5p$ excitation, the product of $P_{4s}(r)$ and $P_{5p}(r)$ switches signs near $8a_0$. Thus, when $K \rightarrow 0$, the two regions partially cancel, leading to a small optical oscillator strength. But as $K$ is increased, at a particular value of $K$, $j_t(Kr)$ switches signs near the node at $8a_0$, such that the two regions now add together leading to a resonant enhancement in the generalized oscillator strength. Ultimately then, the enhancement of the $1s_5 \rightarrow 3p_9$ excitation cross section can be traced to the fact that for $4s \rightarrow 5p$ excitation the $5p$ radial wave function has an extra node.

Stauffer and his co-workers have recently calculated excitation cross sections out of the metastable levels into the levels of $np^5(n+1)p$ configurations for Ne, Ar, Kr, and Xe by means of the relativistic distorted-wave (RDW) method [8]. Of particular relevance is their choice of expressing the target wave functions in terms of the $j$-$j$ coupling basis which clearly delineates the roles of the core angular momentum in the excitation processes and provides a linkage between mathematical formalism and physical description. Since the RDW results for $np^5(n+1)s \rightarrow np^5(n+1)p$ cross sections support the $f_{ij}$ scaling, a similar calculation for the $\mathrm{Ar}(3p^5 4s \rightarrow 3p^5 5p)$ excitations similar to those in Ref. [8] should be most helpful in advancing this simple Born-based analysis to a more refined level.

### C. Comparison to other results

There has been little work published on the $\mathrm{Ar}(3p^5 4s \rightarrow 3p^5 5p)$ excitation cross sections. The only published theoretical calculations for these cross sections have been the configuration averaged Born values mentioned in the last section [25]. Since the individual cross sections do not scale with oscillator strengths, there is no easy way to apportion the configuration averaged values into individual cross sections that can be compared to our measurements. In the absence of any other theoretical or experimental work on $\mathrm{Ar}(3p^5 4s \rightarrow 3p^5 5p)$ metastable excitation cross sections, we compare our results to $\mathrm{K}(4s \rightarrow 5p)$ and $\mathrm{Ar}(3p^5 4s \rightarrow 3p^5 5p)$ ground state excitation cross sections.

As mentioned in the Introduction, the excitation of alkali atoms is similar to the excitation of metastable rare-gas atoms without the dependence on $J$ introduced by the partially empty $np^5$ core in the rare gases. Thus, it is enlightening to compare the excitation cross sections for metastable excitation of the $\mathrm{Ar}(3p^5 4p)$ and $\mathrm{Ar}(3p^5 5p)$ levels with the excitation cross sections of the potassium atom, namely, those into the $\mathrm{K}(4p)$ and $\mathrm{K}(5p)$ levels. Phelps *et al.* found that the direct cross section into the $4p$ level at 10 eV was $47 \times 10^{-16}$ cm$^2$, whereas the cross section into the $5p$ level was $2.0 \times 10^{-16}$ cm$^2$ [3]. These are approximately double the corresponding $\mathrm{Ar}(1s_5 \rightarrow 2p_9)$ and $\mathrm{Ar}(1s_5 \rightarrow 3p_9)$ cross sections measured in our experiments (23 and $1.0 \times 10^{-16}$ cm$^2$). With optical oscillator strengths of 1.02 and 0.0095, respectively, for the $\mathrm{K}(4s\text{-}4p)$ and $\mathrm{K}(4s\text{-}5p)$ transitions, there is also a similar breakdown in the simple Born-Bethe scaling between the $\mathrm{K}(4s \rightarrow 4p)$ and $\mathrm{K}(4s \rightarrow 5p)$ cross sections. Without the extra level structure of Ar, which permits multiple tests of the oscillator strength scaling relation within the same $5p$ manifold, the breakdown of this scaling relationship in K is not as obvious. The measured $\mathrm{K}(5p)$ excitation function is also noticeably more peaked in the 0–15 eV range than the $\mathrm{K}(4p)$ excitation function, much as the dipole-allowed $\mathrm{Ar}(3p^5 5p)$ excitation functions are more peaked than the corresponding dipole-allowed $\mathrm{Ar}(3p^5 4p)$ excitation functions.

In comparison to the wide variation in peak excitation cross sections into the various $3p^5 5p$ levels due to excitation from the metastable levels, the peak excitation cross sections into levels of the $3p^5 5p$ configuration from the ground state exhibit much less variation. At 20 eV the ground state apparent cross sections into the $3p^5 5p$ levels differ at most by a factor of 2.5, with all the values in the range from 9 to 24 $\times 10^{-19}$ cm$^2$ [15]. In comparison, the peak apparent cross sections out of the $1s_5$ metastable level into the $3p^5 5p$ levels differ by up to a factor of 60, with values between 0.02 and $1.2 \times 10^{-16}$ cm$^2$. As was observed previously for the $3p^5 4p$ levels, some of the smallest differences between ground state and metastable state excitation cross sections occur for the $J=0$ levels ($3p_1$ and $3p_5$).

### D. Applications

The wide variation of the $Q(m \rightarrow f)/Q(g \rightarrow f)$ ratio for the $\mathrm{Ar}(3p^5 4p)$ levels has led to many applications in the field of

optical plasma diagnostics. In a low-temperature plasma containing a small fraction of metastable atoms, a given level $f$ in the $2p_x$ series can be populated by an inelastic collision of a ground state atom with a "high" energy electron, or an inelastic collision with a metastable atom and a "low" energy electron. For sufficiently large metastable number densities, some levels such as $\mathrm{Ar}(2p_9)$ are populated mostly through the second route, while other levels such as the $\mathrm{Ar}(2p_1)$ are mostly populated by ground state excitation. Thus, measurements of emission intensities from the various $\mathrm{Ar}(2p_x)$ levels provide an effective means to study the electron energy distribution function and also the metastable atom density [29,30].

When Ar is added as trace addition to a plasma, the large $2p_x$ metastable cross sections have been found to be excellent probes of plasma properties even with low metastable concentrations [31]. For a pure Ar plasma, or plasmas with a large Ar partial pressure, however, the metastable density may be high enough to lead to substantial reabsorption of $3p^54p \rightarrow 3p^54s$ transitions [32]. Such radiation trapping may limit the usefulness of $\mathrm{Ar}(2p_x \rightarrow 1s_y)$ emissions as a plasma diagnostic. In these situations the present $\mathrm{Ar}(3p_x \rightarrow 1s_y)$ may prove useful. Owing to the substantially smaller optical oscillator strengths $[O(10^{-3})$ versus $O(10^{-1})]$, and shorter wavelengths (~400 nm versus ~800 nm), the reabsorption cross sections for the $3p_x \rightarrow 1s_y$ transitions are approximately three orders of magnitude smaller than those in the $2p_x \rightarrow 1s_y$ transition array. While the emission intensities from the $3p_x$ levels are smaller than those from the $2p_x$ levels, the difference is only about one order of magnitude.

The 419.8 nm and 420.1 nm pair of emission lines, in particular, provide an excellent probe of plasma properties [33]. The 419.8 nm emission arises from the $J=0$ $3p_5$ level and has a peak optical-emission cross section due to excitation from the $1s_5$ metastable level of only $0.33 \times 10^{-17}$ cm$^2$, whereas the 420.1 nm line arising from the $J=3$ $3p_9$ has a much larger emission cross section of $1.3 \times 10^{-17}$ cm$^2$. In contrast, the peak excitation cross sections *out of the ground state* for the two levels are almost equal, namely, 29 and $33 \times 10^{-16}$ cm$^2$ for the 419.8 and 420.1 nm emission lines, respectively [18]. Due to the nearly equal ground state cross sections and similar excitation thresholds, the intensity ratio of the two emission lines is virtually independent of the electron temperature in the absence of a metastable contribution to the excitation process. Due to the unequal metastable excitation cross sections, however, with the inclusion of excitation of metastable atoms by low-energy electrons the 420.1 nm emission line should be dramatically increased. Assuming the better than 0.3 nm resolution needed to resolve the pair of lines is not too large a problem, the close spacing does eliminate many calibration uncertainties in comparing intensities at drastically different wavelengths.

## V. CONCLUSIONS

The study of electron excitation from the metastable levels into the $3p^55p$ levels of Ar has fulfilled our dual goals of probing into the basic physics, as well as exploring potential technological applications. In the rare gas series, excitation into $\mathrm{Kr}(4p^55p)$ and $\mathrm{Xe}(5p^56p)$ levels exhibited dramatically different cross sections from the two metastable levels depending on whether the excitation process from the metastable level is core preserving or core changing. The validity of $j_c$ as a good quantum number breaks down for the lighter rare gases, so this core propensity rule does not apply to metastable excitation cross sections for $\mathrm{Ar}(3p^54p)$ and $\mathrm{Ne}(2p^53p)$. The present case of $\mathrm{Ar}(3p^55p)$ provides a new perspective. Here the $3p^5$ core is not so much disturbed by the outer electron $(5p)$ as in the lower $3p^54p$ configuration, thus $j_c$ is now expected to be closer to a good quantum number. Our $3p^54s \rightarrow 3p^55p$ experimental cross sections, however, demonstrate only a partial pattern of core propensity. This may be due to the fact that while $j_c$ is now better defined for the $3p^55p$ final state, it is still ill-defined for the metastable $3p^54s$ initial state. Excitation cross sections out of the ground state, for which $j_c$ is undefined, also show little variation with the core angular momentum of the final state [4]. Another finding is that the cross sections within the $\mathrm{Ar}(3p^55p)$ group no longer track with the oscillator strength in contrast to the general trend observed in the $np^5(n+1)p$ series of all four atoms [4,8]. On the application side the $\mathrm{Ar}(3p^55p \rightarrow 3p^54s)$ emission lines feature prominently in the visible glow of argon plasmas, hence the cross sections for excitation into the $\mathrm{Ar}(3p^55p)$ levels reported in this paper play important roles in plasma diagnostics.

## ACKNOWLEDGMENT

Support by the National Science Foundation is gratefully acknowledged.

[1] J. E. Chilton, J. B. Boffard, R. S. Schappe, and C. C. Lin, Phys. Rev. A **57**, 267 (1998).
[2] J. B. Boffard, G. A. Piech, M. F. Gehrke, L. W. Anderson, and C. C. Lin, Phys. Rev. A **59**, 2749 (1999).
[3] J. O. Phelps, J. E. Solomon, D. F. Korff, C. C. Lin, and E. T. P. Lee, Phys. Rev. A **20**, 1418 (1979).
[4] J. B. Boffard, R. O. Jung, L. W. Anderson, and C. C. Lin, Adv. At., Mol., Opt. Phys. **54**, 319 (2006).
[5] G. A. Piech, J. B. Boffard, M. F. Gehrke, L. W. Anderson, and C. C. Lin, Phys. Rev. Lett. **81**, 309 (1998).
[6] R. O. Jung, T. E. Stone, J. B. Boffard, L. W. Anderson, and C. C. Lin, Phys. Rev. Lett. **94**, 163202 (2005).
[7] R. O. Jung, J. B. Boffard, L. W. Anderson, and C. C. Lin, Phys. Rev. A **72**, 022723 (2005).
[8] R. Srivastava, A. D. Stauffer, and L. Sharma, Phys. Rev. A **74**, 012715 (2006).
[9] A. Dasgupta, M. Blaha, and J. L. Giuliani, Phys. Rev. A **61**, 012703 (1999); **65**, 039905(E) (2002)].

[10] A. Dasgupta, K. Bartschat, D. Vaid, A. N. Grum-Grzhimailo, D. H. Madison, M. Blaha, and J. L. Giuliani, Phys. Rev. A **65**, 042724 (2002).
[11] K. Bartschat and V. Zeman, Phys. Rev. A **59**, R2552 (1999).
[12] R. S. Van Dyck, C. E. Johnson, and H. A. Shugart, Phys. Rev. A **5**, 991 (1972).
[13] R. O. Jung, T. E. Stone, J. B. Boffard, L. W. Anderson, and C. C. Lin, Phys. Rev. A **73**, 022722 (2006).
[14] A. R. Filippelli, C. C. Lin, L. W. Anderson, and J. W. McConkey, Adv. At., Mol., Opt. Phys. **33**, 1 (1994).
[15] T. Weber, J. B. Boffard, and C. C. Lin, Phys. Rev. A **68**, 032719 (2003).
[16] S. Tsurubuchi, T. Miyazaki, and K. Motohashi, J. Phys. B **29**, 1785 (1996).
[17] L. J. Kieffer, At. Data **1**, 121 (1969) [note addenda: **2**, 393 (1971)].
[18] J. B. Boffard, B. Chiaro, T. Weber, and C. C. Lin, At. Data Nucl. Data Tables (to be published).
[19] W. L. Wiese, J. W. Brault, K. Danzmann, V. Helbig, and M. Kock, Phys. Rev. A **39**, 2461 (1989).
[20] J. Z. Klose, J. Opt. Soc. Am. **58**, 1509 (1968).
[21] G. Inoue, D. W. Setser, and N. Sadeghi, J. Chem. Phys. **76**, 977 (1982).
[22] M. J. G. Borge and J. Campos, Physica B & C **119C**, 359 (1983).
[23] Z. Stryla, H. Pobee, W. Schade, and V. Helbig, Phys. Rev. A **41**, 512 (1990).
[24] O. Zatsarinny and K. Bartschat, J. Phys. B **39**, 2145 (2006).
[25] H. A. Hyman, Phys. Rev. A **18**, 441 (1978).
[26] J. B. Boffard, M. L. Keeler, G. A. Piech, L. W. Anderson, and C. C. Lin, Phys. Rev. A **64**, 032708 (2001).
[27] R. D. Cowan, *The Theory of Atomic Structure and Spectra* (University of California Press, Berkeley, 1981).
[28] M. Inokuti, Rev. Mod. Phys. **43**, 297 (1971).
[29] S. A. Moshkalyov, P. G. Steen, S. Gomez, and W. G. Graham, Appl. Phys. Lett. **75**, 328 (1999).
[30] Y. Miyoshi, Z. L. Petrovic, and T. Makabe, J. Phys. D **35**, 454 (2002).
[31] V. M. Donnelly, J. Phys. D **37**, R217 (2004).
[32] M. Böke, G. Himmel, I. Koleva, and M. Schlüter, J. Phys. D **32**, 2426 (1999).
[33] C. A. DeJoseph and V. I. Demidov, J. Phys. B **38**, 3805 (2005).